

Development and Driving Test Evaluation of Electric Vehicle with Wireless In-Wheel Motor

Hiroshi Fujimoto¹⁾

Motoki Sato¹⁾²⁾

Daisuke Gunji³⁾

Takehiro Imura¹⁾

1) The University of Tokyo, 5-1-5 Kashiwanoha, Kashiwa, Chiba, 277-8561 Japan

2) Toyo Denki Seizo K.K., 3-8 Fukuura, Kanazawa-ku, Yokohama, Kanagawa, 236-0004 Japan

3) NSK Ltd., 1-5-50 Kugenumashinmei, Fujisawa, Kanagawa, 251-8501 Japan

Presented at the EVTeC and APE Japan on May 27, 2016

ABSTRACT: A new type of in-wheel motor, which receives electric power by wireless power transfer using magnetic resonance coupling and control signals by wireless communication, in order to avoid the disconnection of power and signal cables have been developed. This system is called Wireless In-Wheel Motor (W-IWM). In this system, it is also possible to directly transmit power to the in-wheel motor without cables from underground coils for dynamic charging in future. This paper introduces the overview and design methods of the W-IWM. We also evaluate the characteristics of the W-IWM when installed on an electric vehicle and demonstrate its effectiveness by a driving test.

KEY WORDS: EV and HV systems, motor drive system, in-wheel Motor, wireless power transfer

1. Introduction

Currently, electric vehicles have been paid attention because of their small environmental impact. Furthermore, an electric motor has a high torque response, compared to an internal combustion engine⁽¹⁾. Actually, the in-wheel motor is one of the best driving system since control performance is exerted to the fullest. When compared with the vehicle motor system, the in-wheel motor system has the following advantages:⁽²⁾⁽³⁾

- Since differential gear and drive shaft are unnecessary, it makes the car design has less constraints; moreover it is also possible to reduce the weight of the whole car body (according to reference (4), the whole drive system will be 36% lighter.) Therefore, energy losses are reduced.
- Motion controllability and vehicle stability are improved because each wheel can be controlled independently.

In general, the in-wheel motor system has the following issues.

- The driving comfort deteriorates because of unsprung weight is increased.
- The power and signal cables might be disconnected from prolonged and repetitive bending as well as small debris impact or freeze in cold regions.

The first problem can be solved by using the anti-dive force control of the in-wheel motor⁽⁴⁾. The second problem has been tackled by increasing durability and reliability of the cable⁽⁵⁾. However, this is still not sufficient to guarantee the safe transmission of input signal and electric power. Therefore, a novel solution consisting in a bidirectional power transmission system between car body and a wheel. A prototype has been built and test runs have been conducted. This structure is called Wireless In-Wheel

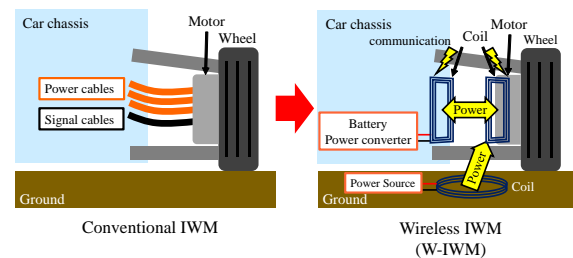


Fig. 1 The concept of W-IWM.

Motor (W-IWM). In this circuit, coils for wireless power transfer and communication system are installed both in the wheel and the car body, thus eliminating the cables in between. The relative position of the power transmitting and receiving coil changes with the movement of the suspension in the actual car body. Consequently, the authors choice is the magnetic resonant coupling for wireless power transfer⁽⁶⁾⁽⁷⁾. Since the W-IWM is capable of both receiving and transmitting power, it also allows for regenerating energy when the vehicle is decelerating. With this technology, dynamic charging in which electric vehicles powered by devices embedded in the highway surface are a definite possibility in future. It is well known that the receiver side coil voltage and current fluctuate because of the variation of either the coils relative position or the load⁽⁸⁾. Furthermore, in the case of a constant power load, the secondary side load voltage is unstable⁽⁹⁾. Therefore, controlling the voltage or the current by converters in both transmitter and receiver side is necessary for the good operation of the W-IWM.

In addition, metallic parts such as the suspension arm around



(a) FPEV4-Sawyer (b) First trial unit

Fig. 2 Test vehicle and prototype unit.

Table 1 Target value of the vehicle performance and the first prototype goal.

	Final target	First target
Number of in-wheel motor	4	2
Rated output power	48 kW	6.6 kW
Rated wheel torque	1300 Nm	475 Nm
Dynamic charging from road	possible	N/A

the in-wheel motor are present in the vehicle. Since the magnetic resonant coupling method is adopted, these metallic parts greatly affect the power transmission efficiency.

In order to minimize the adverse effect of these metals, designing both the arrangement and the shape of the coils are necessary. Choosing suitable magnetic materials for the coils is important, too.

In this paper, the development of wireless in-wheel motor by magnetic resonant coupling method is presented. This paper describes the control of the structure and the power conversion circuit of the prototype unit to be mounted for the experiment on electric vehicles. In addition, the running test results with the electric vehicle equipped with a prototype unit are reported.

2. Wireless In-Wheel Motor.

2.1. Expected vehicle performance.

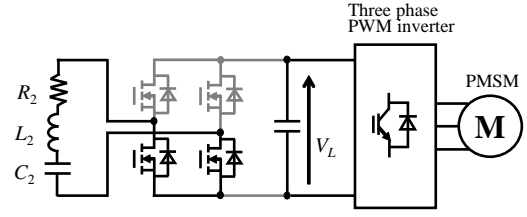
The in-wheel motor lack of power and signal cables is shown in in Fig. 1.

The vehicle for the experiment, FPEV4-Sawyer, has been developed in the authors' laboratory at the University of Tokyo, as shown in Fig. 2(a).

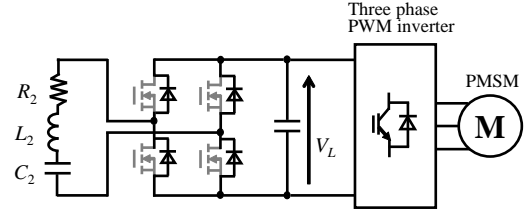
This vehicle has a replaceable sub-unit configuration for both the front and rear wheels, consequently it can test and compare a wide variety of drive units on the same platform. The sub-unit in the prototype is shown in Fig. 2(b). In Table 1, are reported the vehicle specifications. The final target output power is 48 kW with the four-wheel, while the first trial output power is 6.6 kW for the two rear wheels. In other words, the aim is a continuous rated output power of 3.3 kW per wheel, a necessary parameter for designing a large power transmission control and the coils. In addition, considering the space between the in-wheel motor and the body necessary to the suspension stroke, the gap between the transmitting and receiving coils is set to 100 mm.

2.2. Wireless power transmission of the magnetic resonant coupling method

In the wireless power transmission by magnetic resonant cou-



(a) Short mode



(b) Rectification mode

Fig. 4 Operating pattern of the receiver circuit.

pling method adopted in the W-IWM, matching the resonant frequency of the LC circuit used in the coils is mandatory. The operation point angular frequency of the primary-side inverter is

$$\omega_0 = \frac{1}{\sqrt{L_1 C_1}} = \frac{1}{\sqrt{L_2 C_2}}, \quad (1)$$

where L_1 and L_2 as primary and secondary coil inductance, respectively; similarly, C_1 and C_2 are the primary and secondary coil resonant capacitors. In this paper the coils and their relative resonant capacitors form a system, referred to as resonator. Furthermore, the vehicle body side becomes the primary side (power transmission side) and the in-wheel motor is considered the secondary side (power receiving side). Finally, the resonant frequency $f_0 (= \omega_0/2\pi)$, is assumed to be 85 kHz, according to the international standards for static wireless power transmission to electric vehicles⁽¹¹⁾.

2.3. Technical challenges.

To achieve a fully functional and competitive W-IWM, there are some technical challenges such as the following.

- Designing the electric conversion circuits.
- Developing control for secondary DC-link voltage without high speed communication system between primary side and secondary side .
- Achieving bi-directional electric power transfer.
- Fabricating the coils suitable for high efficiency and high power transmission.

This paper shows solutions against above mentioned.

3. Basic structure and control method of power conversion circuits.

A circuit structure of W-IWM is shown in Fig. 3. In many previous papers about wireless power transfer, secondary side components consisted in full bridge rectification circuit and DC/DC converter⁽¹²⁾. However, the secondary circuits must be placed in limited space (i.e. into a wheel). In addition, the secondary side

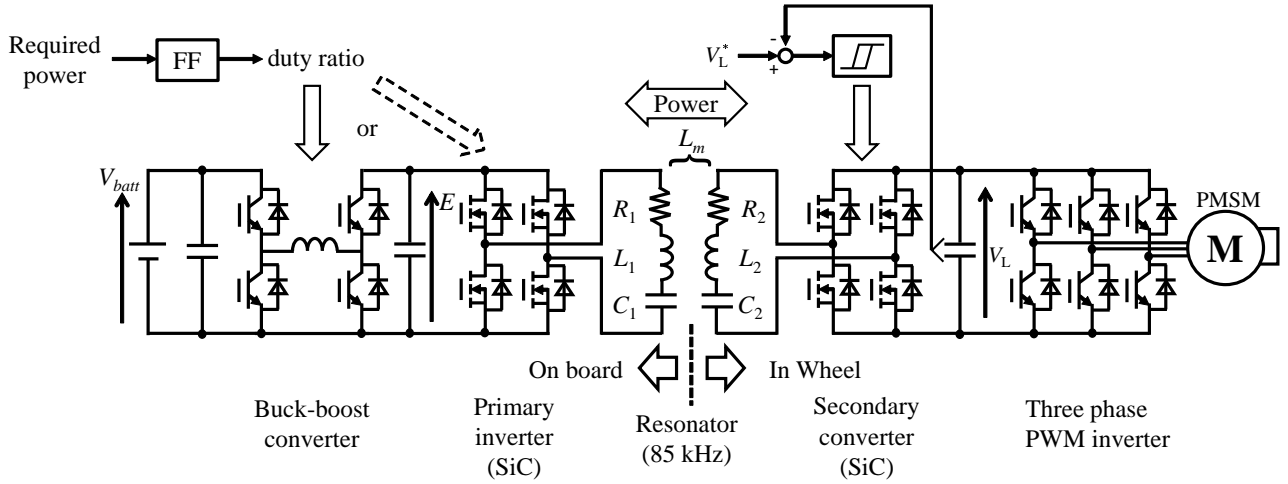


Fig. 3 Circuit structure of wireless in-wheel motor.

rectifier works as a transmitting inverter during regeneration from braking. Therefore, W-IWM circuit becomes as below. The primary circuit includes a bi-directional buck-boost chopper and full bridge circuit. The battery voltage is converted to suitable voltage and fed to full bridge inverter. The inverter output is an AC square wave with the same frequency of the resonators (i.e. the same as resonant frequency). The electric power of the AC square wave is transferred to secondary side by using magnetic resonant coupling. Transmitted power is then rectified to DC power by full bridge circuit. Finally, the DC-link voltage is converted with 3 phase inverter, which drives the permanent magnetic synchronous motor.

3.1. Feedforward power control in primary side.

Primary side power is feedforward controlled. If the secondary DC-link voltage is controlled and stable, the secondary DC-link current fluctuates in response to the motor output power. That is, motor output circuit is considered as an equivalent variable resistance changing along the motor output power. It is known that transmitted power varies accordingly to the load resistance in magnetic resonant coupling⁽⁸⁾. Therefore, the controller calculates the power necessary to the secondary side motor, based on motor torque and motor speed information. Moreover, the feedforward controller regulates the primary side inverter output voltage based on calculated power, as mentioned before. The number of revolutions of the synchronous motor, measured with an encoder, is feedback controlled from primary side by Bluetooth communication. Since the fluctuation of the number of revolutions is slow enough compared with latency of LSI for Bluetooth communication, high speed communication is not mandatory for feedback control.

3.2. Feedback voltage control of DC-link in secondary side.

It is known that in case of constant power load, the behavior of DC-link voltage will be unstable⁽⁹⁾. Therefore, DC-link voltage stabilization based on feedback control is required. It should be

noted that the feedback control described in this paper is completely closed in the secondary side to avoid high speed communication between primary side and secondary side. As a control method to keep the V_L constant by using only the secondary side circuit, two methods have been considered: hysteresis comparator and synchronous rectification. However, in this paper, only the hysteresis comparator in the secondary converter is covered. In case of DC-link voltage control by hysteresis comparator as shown in Fig. 4, the devices in the high side are always OFF, while low side switching devices are controlled and turned ON and OFF. Lower threshold voltage V_{low} and upper threshold voltage V_{up} of hysteresis comparator are defined as

$$V_{low} = V_L^* - \Delta V, \quad (2)$$

$$V_{up} = V_L^* + \Delta V. \quad (3)$$

V_L^* is the DC-link voltage reference, ΔV is the hysteresis band.

Fig. 5 shows the magnified view of DC-link voltage V_L . When V_L reaches the V_{up} , the switching devices of the low side are ON. The secondary side coil terminal are shorted and the system is in "Short mode" as shown in Fig. 4(a). In this state, the power transmitted to the load is zero and the DC-link voltage V_L decreases.

On the other hand, when V_L is lower than the V_{low} , the switching devices of the lower arm are OFF. The secondary side circuit is in "Rectification mode" as shown in Fig. 4(b). The power is transmitted to the load and the DC-link voltage will rise if the transmitted power is greater than the load power.

The low side switching pattern forces the DC-link voltage V_L in secondary side to be always in the vicinity of the reference V_L^* , as shown in Fig. 5.

3.3. Power regeneration operation.

The circuit topology of the unit for wireless power conversion is symmetrical in the primary and secondary side; this means that the power regeneration process is simple to operate. Power is regenerated from the motor, when the secondary-side DC link

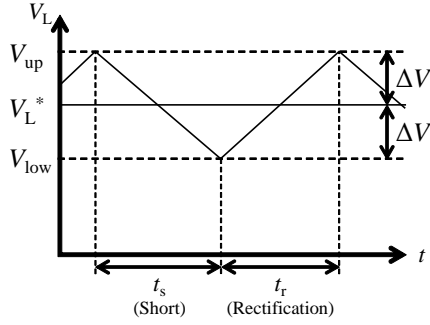


Fig. 5 DC-link voltage waveform.

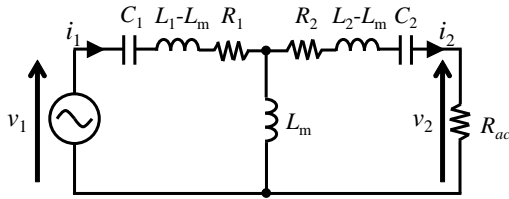


Fig. 6 Simple equivalent circuit of wireless power transmission unit.

voltage V_L is equal to or greater than a threshold value. At the same time, command signal is send to the primary side in order to make the inverter operate as a diode bridge rectifier. This configuration can achieve the power regeneration from the secondary side to the primary side.

4. Design of wireless power transfer units.

4.1. Design of the power transmitting and receiving coils.

4.1.1. Designing

This chapter describes an AC power supply of the buck-boost chopper and the PWM inverter of the primary side. When the power factor of the secondary side circuit is assumed to be unity, then the entire load after the rectifying circuit is regarded as a variable pure resistance⁽⁸⁾. Therefore, when the entire equivalent load that is regarded as a pure resistance R_{ac} , the equivalent circuit of the W-IWM can be simplified as Fig. 6. Since the primary inverter frequency is fixed to ω_0 , the voltage ratio A_V and the transmission efficiency η between the coils are represented by

$$A_V = \frac{V_2}{V_1} = j \frac{\omega_0 L_m R_{ac}}{R_1 R_{ac} + R_1 R_2 + (\omega_0 L_m)^2}, \quad (4)$$

$$\eta = \frac{V_2 \bar{I}_2}{V_1 \bar{I}_1} = \frac{(\omega_0 L_m)^2 R_{ac}}{(R_{ac} + R_2) \{R_1 R_{ac} + R_1 R_2 + (\omega_0 L_m)^2\}}. \quad (5)$$

In the efficiency formula of the wireless power transfer (5), R_1 , R_2 , and L_m are parameters depending on the size and number of turns of the coil. Furthermore, L_m changes due to relative position. From the (5), when R_1 are R_2 are smaller or when L_m is higher, the efficiency becomes higher. In general, a larger resonator has bigger L_m and larger R_1 and R_2 . Thus, the size of the coil is determined in consideration of this trade off .

Table 2 Range of parameters in coil design.

	R_1	R_2	L_m
Fig. 7 (a)	0.10~4.0 Ω	1.0 Ω	40 μH
Fig. 7 (b)	1.0 Ω	0.10~4.0 Ω	40 μH
Fig. 7 (c)	1.0 Ω	1.0 Ω	20~60 μH

Table 3 Target parameters of coils.

Parameter of coil	Target
Primary coil resistance R_1	under 1.0 Ω
Secondary coil resistance R_2	1.0 Ω
Mutual inductance L_m	over 40 μH

4.1.2. Target value of the coil parameters.

In this section, the target values of three variables, L_m , R_1 , R_2 , are determined. By varying one variable and keeping fixed the other two, in Fig. 7 the graphics of the efficiency with respect to R_{ac} are presented. In the case of FPEV4-*Sawyer*, when fabricating the coils to be fit into the subframe unit, the calculated parameters are expected to be in the following range: R_1 and R_2 will be between 0.1 and 4.0 Ω while L_m will be from 20 to 60 μH , as shown in Table 2.

From Fig. 7(a) and (c), R_1 and L_m are the most significant contributors to the transmission efficiency. Here, the primary side inverter works as a square-wave inverter to generate a square wave voltage in the coils. Moreover, the coil current becomes sine wave. Then, only the fundamental wave component contributes to real power transmission. The equivalent load resistor R_L can be defined by the fundamental wave rms value V_{21} of the secondary coil voltage and the received power P_2 as

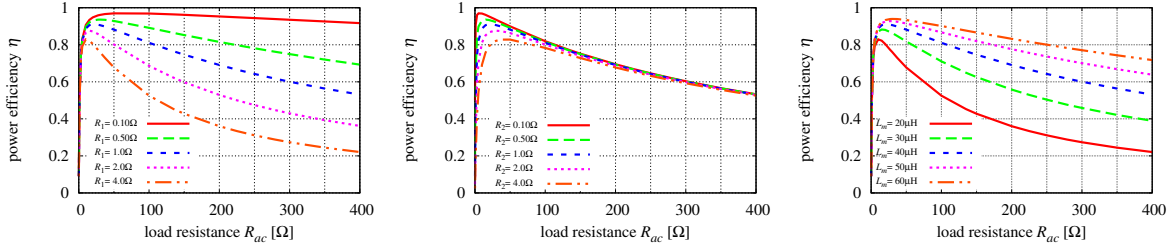
$$R_{ac} = \frac{V_{21}^2}{P_2}. \quad (6)$$

Here, since the devices anti-parallel diode conducts in the rectification mode and the secondary coil voltage is square wave, the relationship between the secondary side DC link voltage V_L and V_{21} can be formulated by using the Fourier series coefficient as

$$V_{21} = \frac{2\sqrt{2}}{\pi} V_L. \quad (7)$$

In this paper, the rated input voltage of the three-phase voltage-type inverter V_L is set to 350 V. Consequently, the desired equivalent load resistance value is achieved when the received power P_2 becomes the rated output 3.3 kW. With that equivalent load resistance of $R_{ac} = 30\Omega$, higher efficiency is especially required in the power order of kW class.

The target value of the transmission efficiency at the rated power output is 90 %. As a condition to achieve this, Fig. 7 shows that the primary coil resistance R_1 must be less than 1 Ω , secondary coil resistance R_2 must be around 1 Ω , and the mutual inductance between coils L_m must be higher than 40 μH , as shown in Table 3.



(a) Transmitting efficiency at the R_1 change. (b) Transmitting efficiency at the R_2 change. (c) Transmitting efficiency at the L_m change.
 Fig. 7 Transmission efficiency at the time of coil parameter variation.

Table 4 Coil parameters

Parameter	Primary	Secondary
Coil resistance $R_{1,2}$	0.411 Ω	0.382 Ω
Coil inductance $L_{1,2}$	260 μH	223 μH
Capacitance $C_{1,2}$	13.5 nF	15.7 nF
Size	218 x 350 mm	218 x 300 mm
Mutual inductance L_m	48.6 μH (gap: 100 mm)	
Resonance frequency	85.0 kHz	

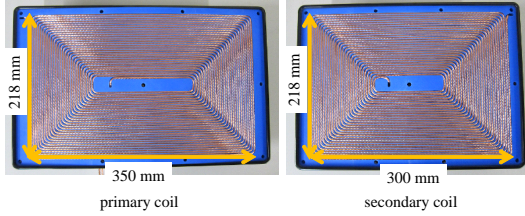


Fig. 8 Overview and size of the resonator coils.

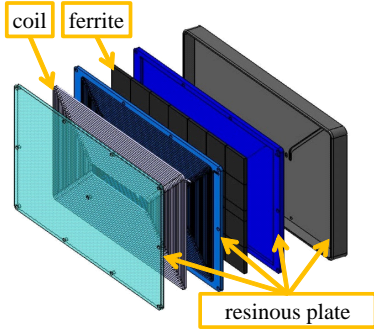


Fig. 9 The configuration of the resonator coils.

4.2. Fabrication of the resonator coils.

The material and shape of the resonator coils are determined from the following considerations .

- The coil shape should be planar because of the limited space of installation where the wheel is surrounded by metallic parts.
- A ferrite plate is placed on the back of both coils in order to reduce iron losses caused by the surrounding metallic parts and to increase the coil mutual inductance.
- Litz wire is used to reduce the skin effect and improve thermal stability.

The parameters of the fabricated coils are shown in Table 4.

When they are installed in the experimental vehicle, the primary and secondary coils must be fixed in the vehicle body and in the wheel, respectively. In order to protect the coils from water and dust, it is necessary to cover them; thus, the coils and the ferrite plate are inserted in a compact box module with a resin cover, as shown in Fig. 8 and Fig. 9.

4.3. Primary side (vehicle body side) unit configuration.

The primary side circuit is located in the vehicle body and is composed of a buck-boost chopper and a full bridge circuit. IGBTs are chosen as the switching devices of the chopper circuit. On the other hand, for high switching frequency operation at 85 kHz, the full bridge circuit uses SiC MOSFETs. In the power conversion circuit on the primary side, the aforementioned feed-forward control is performed. There is two-degree-of-freedom to control the primary voltage as follows.

- 1)Controlling the primary side DC voltage with the buck-boost chopper.
- 2)Controlling the inverter duty cycle.

Although the buck-boost chopper does not need in the case of 2), it is installed to compare the two methods in future. In this paper, much simpler method of 1) is applied, where the buck-boost chopper controls the voltage amplitude and the duty cycle of the inverter is fixed to 0.5 which means square wave inverter operation.

4.4. Secondary side (in-wheel motor side).

The secondary side is an electro-mechanical integrated structure for mounting the full bridge circuit, the three-phase inverter, the permanent magnet synchronous motor, and the mechanical brake all within a wheel. Again, for high frequency operation at 85 kHz, the SiC MOSFETs are also selected as the switching devices of the full bridge circuit. The motor-drive inverter uses IGBTs, and its switching frequency is 6 kHz.

The motor speed is reduced by the hub bearing built-in reduction gear (reduction ratio 4.2) and becomes the final wheel output. The prototyped secondary side structure is shown in Fig. 10.

5. Experiment

5.1. Efficiency evaluation on bench test.

In Fig. 11, an overview of the bench test setup is shown. The voltage source is a three-phase voltage of 200 Vrms and DC input

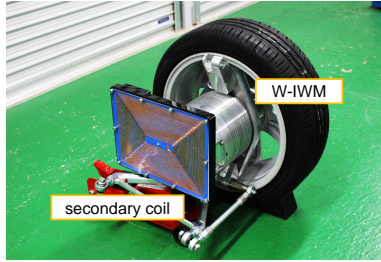


Fig. 10 Secondary side (in-wheel motor side)

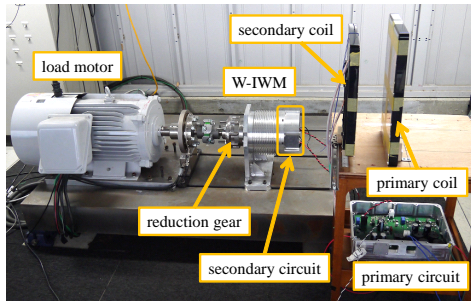


Fig. 11 Bench test set up

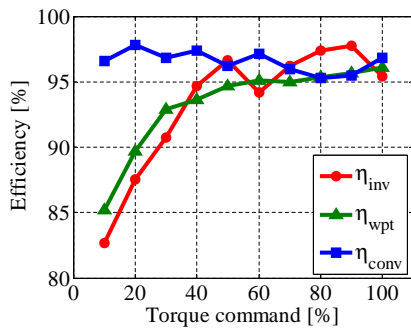


Fig. 12 Each converter efficiency at rated speed (135 r/min)

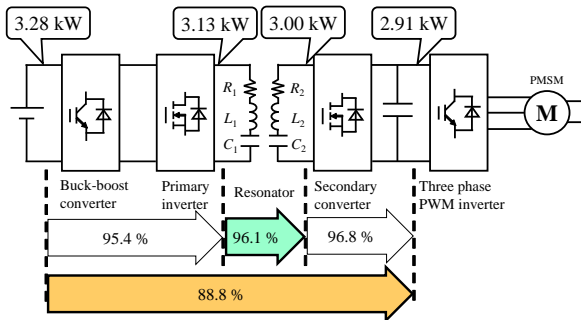
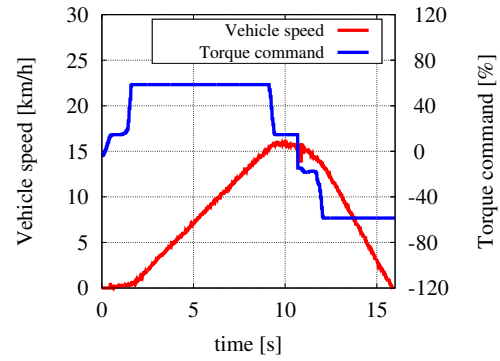


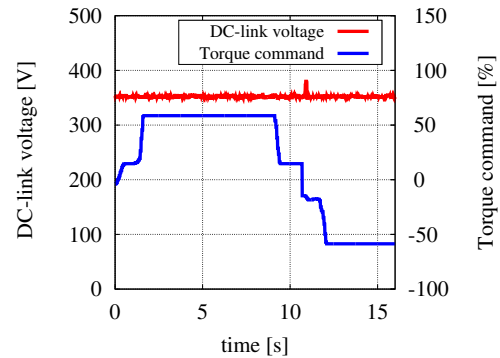
Fig. 13 W-IWM efficiency at rated power

is obtained by a rectification circuit. This rectified voltage source substitutes a battery source. The gap between two coils is 100 mm, which is the same in the experiment vehicle.

In Fig. 12, the efficiency of each converter is shown when the rotational speed is constant at 135 rpm and the torque changes by the command. When the output power is large, each converter efficiency is higher than 95 [%]. However, if the output power is small, the primary side inverter efficiency η_{inv} and the coil trans-



(a) Vehicle speed and torque command



(b) DC-link voltage and torque command

Fig. 14 Running test 1 of W-IWM.

mission efficiency η_{wpt} are reduced, but the total loss is small in the lower power condition.

The efficiency of each converter and the measurement of the power in nominal conditions is shown in Fig. 13. In this case, the rotational speed of the motor load is also 135 rpm, while the torque command is 100%. The efficiency from primary voltage source to secondary DC-link voltage is 88.8 %. Therefore, the effectiveness of W-IWM is verified because its performance reaches our target.

5.2. Driving experiment

Two units of W-IWMs have been equipped to rear wheels of the actual vehicle and running tests have been conducted. The tests results are shown Fig. 14 and Fig. 15. The torque command value to the W-IWM is decided by the driver when operating the accelerator pedal of the experimental vehicle and transmitted to the W-IWM by CAN network and the Bluetooth communication.

Fig. 14(a) and Fig. 15(a) show the vehicle speed and W-IWM torque command value. When the regenerative torque increases, the figures show that the vehicle decelerates quickly and gradually, respectively, according to the driver's command. Fig. 14(b) and Fig. 15 (b) show that even when the command torque is varied, the secondary side DC-link voltage is constantly kept at 350 V by the control. These figures confirm that the load stabilization has been successful by the developed secondary side feedback control while the DC link voltage is unstable without this control⁽⁹⁾. However, because of the Bluetooth communication de-

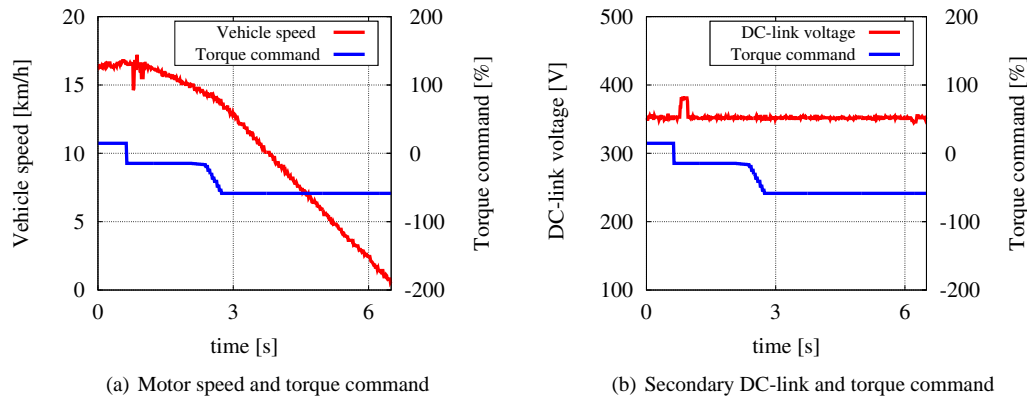


Fig. 15 Running test 2 of W-IWM.

lay, a period of battery-to-motor powering operation has been observed during regenerative braking. This delay caused the small increase of the secondary DC-link voltage. However, this can be attenuated by controlling the motor current, without activating over-voltage protection.

6. Conclusion

In this paper, the W-IWM in which power and signal are transferred using the wireless power transmission and wireless communication has been developed in order to avoid cable disconnections caused by harsh environment. A design method has been described and its validity has been confirmed by actual vehicle test. As for future works, wireless power transfer from coil embedded in the road to the W-IWM is considered. Furthermore, the power-up of the W-IWM by increasing its specification is planned.

Acknowledgment

The research presented in this paper was funded in part by the Ministry of Education, Culture, Sports, Science and Technology grant (No. 26249061). The authors would like to express their deepest appreciation to the Murata Manufacturing Co., Ltd. for providing the laminated ceramic capacitors (U2J characteristics) used in these experiments.

References

- (1) Y. Hori: "Future Vehicle Driven by Electricity and Control Research on Four Wheel Motored "UOT Electric March II"", IEEE Trans. IE, Vol. 51, No. 5, pp. 954–962 (2004)
- (2) S. Harada, H. Fujimoto: "Range extension control system for electric vehicles during acceleration and deceleration based on front and rear driving-braking force distribution considering slip ratio and motor loss", 39th Annual Conference of the IEEE Industrial Electronics Society (IECON), pp. 6626–6631 (2013)
- (3) S. Murata: "Vehicle Dynamics Innovation with In-Wheel Motor," Proc. JSAE EVTeC'11, 20117204, Yokohama, (2011).
- (4) Naoya Ochi, Hiroshi Fujimoto and Yoichi Hori: "Proposal of Roll Angle Control Method Using Positive and Negative Anti-dive Force for Electric Vehicle with Four In-wheel Motors", IEEE International Conference on Mechatronics, Vicenza, Italy, pp.815–820, (2013)
- (5) Toyota Motor Corporation, P2012–223041A 2012. (in Japanese)
- (6) A. Kurs, A. Karalis, R. Moffatt, J. D. Joannopoulos, P. Fiske, and M. Soljacic: "Wireless Power Transfer via Strongly Coupled Magnetic Resonances", in Science Express on 7 June 2007, Vol. 317, No. 5834, pp. 83–86 (2007)
- (7) T. Imura, H. Okabe, T. Uchida, and Y. Hori: "Flexibility of Contactless Power Transfer using Magnetic Resonance Coupling to Air Gap and Misalignment for EV", IEEE Electric Vehicle driven on Electric Vehicle Symposium 24, (2009).
- (8) M. Kato, T. Imura, and Y. Hori: "The Characteristics when Changing Transmission Distance and Load Value in Wireless Power Transfer via Magnetic Resonance Coupling", IEEE Telecommunications Energy Conference INTELEC (2012)
- (9) D. Gunji, T. Imura, H. Fujimoto, "Fundamental Research on Control Method for Power Conversion Circuit of Wireless In-Wheel Motor using Magnetic Resonance Coupling", IEEEJ Transaction on Industry Applications, Vol. 135, No. 3 pp.182–191 (2015)
- (10) H. Fujimoto, T. Miyajima, and J. Amada: "Development of Electric Vehicle with Variable Drive Unit System", International Electric Vehicle Technology Conference & Automotive Power Electronics Japan 2014 (2014)
- (11) SAE International: "Wireless charging advances with selection of 85-kHz charging frequency", <http://articles.sae.org/12647/> (2013)
- (12) W. Zhong and S. Y. R. Hui: "Maximum Energy Efficiency Tracking for Wireless Power Transfer Systems", Power Electronics, IEEE Transactions on (2014)